

siunitx2012/07/222.5gAcomprehensive(SI)unitspackage
Optimization-based coupling of local and nonlocal models: Applications to peridynamics¹

Marta D’Elia¹, Pavel Bochev¹, David Littlewood¹, Mauro Perego¹

¹Center for Computing Research, Sandia National Laboratories, Albuquerque, NM
mdelia,pbboche,djlittl,mperego@sandia.gov

Abstract

1 Introduction

Nonlocal continuum theories such as peridynamics [?] and physics-based nonlocal elasticity [?] can capture strong nonlocal effects due to long-range forces at the mesoscale or microscale. For problems where these effects cannot be neglected, nonlocal models are more accurate than classical Partial Differential Equations (PDEs) that only consider interactions due to contact. However, the improved accuracy of nonlocal models comes at the price of a computational cost that is significantly higher than that of PDEs.

The goal of Local-to-Nonlocal (LtN) coupling methods is to combine the computational efficiency of PDEs with the accuracy of nonlocal models. LtN couplings are imperative when the size of the computational domain or the extent of the nonlocal interactions are such that the nonlocal solution becomes prohibitively expensive to compute, yet the nonlocal model is required to accurately resolve small scale features (such as crack tips or dislocations that can affect the global material behavior). In this context, the main challenge of a coupling method is the stable and accurate merging of two fundamentally different mathematical descriptions of the same physical phenomena into a physically consistent coupled formulation.

1.1 Structure of the chapter

This chapter is organized as follows. In Section 2 we present an abstract framework of optimization-based coupling (OBC) methods. In Section 3 we introduce the static peridynamics and the local elasticity state models and describe their properties. In Section 4 we specialize the OBC approach to the state models and in Section 5 we describe its fully discrete formulation; here we also review the discretization scheme for static peridynamics. Finally, in Section 6 we demonstrate the consistency and efficiency of the coupling method through several numerical tests using Sandia’s agile software components toolkit.

1.2 Local to nonlocal coupling methods for continuum mechanics

The promise of improved physical fidelity at a lower computational cost has attracted significant attention to the coupling of nonlocal and local material models in continuum mechanics. The bulk of the existing methods though, is based on some form of *blending* of the two material models. This blending can involve the energies of the two models, their force balance equations, or even their material properties. We describe three examples that are representative of these types of couplings.

The extension of the Arlequin method [?] to LtN couplings of continuum mechanics models by Han and Lubineau [?] is an example of an *energy-blending* approach. Their method splits the domain into a nonlocal subdomain, where the nonlocal effects are pronounced, and an overlapping local subdomain, where such effects are negligible. The intersection of these

properties of both the local and nonlocal models in the overlap regions. Second, they treat the kinematic compatibility between the models, e.g., the equality of their displacements over a suitable interface, as a constraint in a way that is reminiscent of classical domain decomposition methods. In the next section we describe a general Optimization-Based Coupling (OBC) strategy that differs fundamentally from the blending approaches discussed above and offers some distinct computational and theoretical advantages.

2 Principles of optimization-based couplings

In contrast to the blending methods described earlier, an Optimization-Based Coupling (OBC) strategy treats the coupling condition as an optimization objective, which is minimized subject to the model equations acting independently in their respective subdomains. In so doing OBC reverses the roles of the coupling conditions and the governing equations and keeps the latter separate.

In particular, the coupling of local and nonlocal models is effected by couching the LtN coupling into an optimization problem. The objective is to minimize the mismatch of the local and nonlocal solutions on the overlap of their subdomains, the constraints are the associated governing equations, and the controls are the virtual nonlocal volume constraint and the local boundary condition. This approach is inspired by non-standard optimization-based domain decomposition methods for PDEs [?, ?, ?, ?, ?, ?, ?, ?]. It has also been applied to the coupling of discrete atomistic and continuum models in [?, ?]. This strategy brings about valuable theoretical and computational advantages. For instance, the coupled problem passes a patch test by construction, its well-posedness typically follows from the well-posedness of the constraint equations and its numerical solution only requires the implementation of the optimization strategy as the local and nonlocal solvers for the state equations can be used as black boxes. For this reason we refer to OBC methods as *non-intrusive* as opposed to the coupling methods described in Section 1.2, which are *intrusive* in the sense that their implementation requires modification of the basic governing equations for the local and nonlocal models in the overlap region. In what follows we present an abstract formulation of OBCs.

Let $\mathcal{L}_n : \mathcal{V}_n \rightarrow \mathbb{R}$ be a nonlocal operator that accurately describes the behavior of the material in a bounded body and let $\mathcal{L}_l : \mathcal{V}_l \rightarrow \mathbb{R}$ be a local operator that describes the material well enough where the nonlocal effects are negligible. We recall that the numerical solution of the accurate nonlocal model is computationally expensive, whereas the one of the local model is, in general, affordable. As in the coupling methods described in Section 1.2 we solve the nonlocal model where the nonlocality affects the global material behavior and the local problem everywhere else; the challenge is to couple those models at the interfaces or overlaps of their domains. As explained above, we tackle this by solving an optimization problem where we minimize the difference between the local and nonlocal solutions at the interfaces tuning their values on the virtual boundaries and volumes induced by the domain

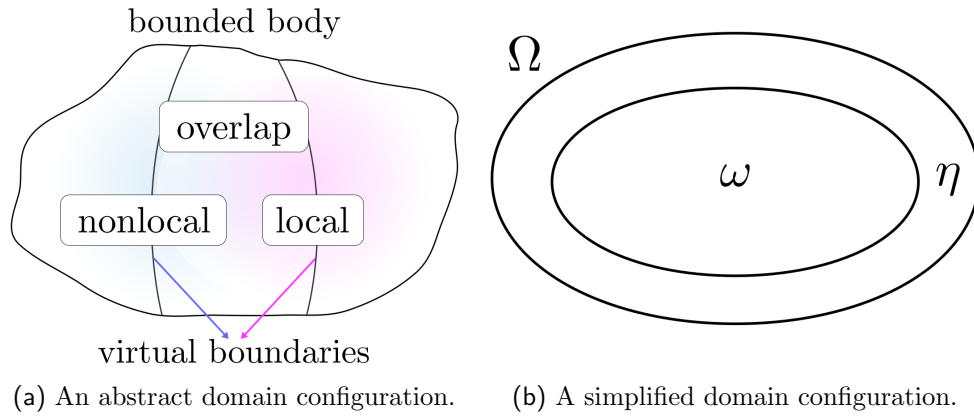


Fig. 1: Illustration of LtN OBC domain configurations for a bonded body Ω and its decomposition into ω and η .

decomposition, see Fig. 1, left. Formally, we state the LtN OBC as follows:

$$\begin{aligned}
 \min_{\mathbf{u}_n, \mathbf{u}_l, \boldsymbol{\nu}_n, \boldsymbol{\nu}_l} \mathcal{J}(\mathbf{u}_n, \mathbf{u}_l) &= \frac{1}{2} \|\mathbf{u}_n - \mathbf{u}_l\|_{*, \text{overlap}}^2 \\
 \text{s.t.} \quad \begin{cases} -\mathcal{L}_n \mathbf{u}_n = \mathbf{b}(\mathbf{x}) & \text{nonlocal domain} \\ \mathbf{u}_n(\mathbf{x}) = \mathbf{g}(\mathbf{x}) & \text{physical n-boundary} \\ \mathbf{u}_n(\mathbf{x}) = \boldsymbol{\nu}_n(\mathbf{x}) & \text{virtual n-boundary} \end{cases} \quad \begin{cases} -\mathcal{L}_l \mathbf{u}_l = \mathbf{b}(\mathbf{x}) & \text{local domain} \\ \mathbf{u}_l(\mathbf{x}) = \mathbf{g}(\mathbf{x}) & \text{physical boundary} \\ \mathbf{u}_l(\mathbf{x}) = \boldsymbol{\nu}_l(\mathbf{x}) & \text{virtual boundary,} \end{cases} \quad (1)
 \end{aligned}$$

where \mathbf{b} is a body force density, $\|\cdot\|_{*, \text{domain}}$ is a suitable norm on a domain, $(\boldsymbol{\nu}_n, \boldsymbol{\nu}_l) \in \mathcal{C}$ (the control space) are the control variables. “N-boundary” stands for nonlocal boundary, usually called interaction volume (rigorously defined in Section 3), that consists of all points outside of the domain that interact with points inside the domain. Thus, the goal of OBC is to find optimal values of the virtual controls $\boldsymbol{\nu}_n$ and $\boldsymbol{\nu}_l$ such that \mathbf{u}_n and \mathbf{u}_l are as close as possible on the overlap and still satisfy the model equations, which play the role of optimization constraints.

Note that this approach is very general and flexible and can be applied to any nonlocal model for continuum mechanics when a suitable local approximation is available. In this chapter we use the OBC technique to combine nonlocal elasticity, described by a static peridynamics model, and classical linear elasticity. Our strategy is based on the recently introduced approaches [?, ?, ?] for local and nonlocal diffusion [?].

2.1 Well-posedness

We present a strategy for proving the well-posedness of (1) for linear operators \mathcal{L}_l and \mathcal{L}_n . Here, without loss of generality, we consider $\mathbf{g} = \mathbf{0}$. We assume that for any pair of controls the constraints in (1) have unique solutions $\mathbf{u}_n(\boldsymbol{\nu}_n)$ and $\mathbf{u}_l(\boldsymbol{\nu}_l)$. We introduce the reduced form of the optimization problem by eliminating the states from (1) and obtaining an optimization problem in terms of $\boldsymbol{\nu}_n$ and $\boldsymbol{\nu}_l$ only:

$$\min_{\boldsymbol{\nu}_n, \boldsymbol{\nu}_l} \mathcal{J}(\boldsymbol{\nu}_n, \boldsymbol{\nu}_l) = \frac{1}{2} \|\mathbf{u}_n(\boldsymbol{\nu}_n) - \mathbf{u}_l(\boldsymbol{\nu}_l)\|_{*,o}^2, \quad (2)$$

where “o” stands for “overlap”. Following the approach used in [?, ?, ?, ?], one can show the well-posedness of (2) by splitting the solution of the state equations into the “harmonic” components $(\mathbf{v}_n(\boldsymbol{\nu}_n), \mathbf{v}_l(\boldsymbol{\nu}_l))$ and the homogeneous components $(\mathbf{u}_n^0, \mathbf{u}_l^0)$ such that they respectively satisfy

$$\left\{ \begin{array}{ll} -\mathcal{L}_n \mathbf{v}_n = \mathbf{0} & \text{nonlocal domain} \\ \mathbf{v}_n = \mathbf{0} & \text{physical n-boundary} \\ \mathbf{v}_n = \boldsymbol{\nu}_n & \text{virtual n-boundary} \end{array} \right. \quad \left\{ \begin{array}{ll} -\mathcal{L}_l \mathbf{v}_l = \mathbf{0} & \text{local domain} \\ \mathbf{v}_l = \mathbf{0} & \text{physical boundary} \\ \mathbf{v}_l = \boldsymbol{\nu}_l & \text{virtual boundary,} \end{array} \right. \quad (3)$$

and

$$\left\{ \begin{array}{ll} -\mathcal{L}_n \mathbf{u}_n^0 = \mathbf{b} & \text{nonlocal domain} \\ \mathbf{u}_n^0 = \mathbf{0} & \text{n-boundary} \end{array} \right. \quad \left\{ \begin{array}{ll} -\mathcal{L}_l \mathbf{u}_l^0 = \mathbf{b} & \text{local domain} \\ \mathbf{u}_l(\mathbf{x}) = \mathbf{0} & \text{boundary.} \end{array} \right. \quad (4)$$

In terms of the components $\mathbf{u}_n = \mathbf{v}_n + \mathbf{u}_n^0$ and $\mathbf{u}_l = \mathbf{v}_l + \mathbf{u}_l^0$, the objective function and the Euler-Lagrange equations are given by

$$\mathcal{J}(\boldsymbol{\nu}_n, \boldsymbol{\nu}_l) = \frac{1}{2} \|\mathbf{v}_n(\boldsymbol{\nu}_n) - \mathbf{v}_l(\boldsymbol{\nu}_l)\|_{*,o}^2 + \frac{1}{2} \|\mathbf{u}_n^0 - \mathbf{u}_l^0\|_{*,o}^2 + (\mathbf{v}_n(\boldsymbol{\nu}_n) - \mathbf{v}_l(\boldsymbol{\nu}_l), \mathbf{u}_n^0 - \mathbf{u}_l^0)_{*,o},$$

and

$$Q(\boldsymbol{\sigma}_n, \boldsymbol{\sigma}_l; \boldsymbol{\beta}_n, \boldsymbol{\beta}_l) = F(\boldsymbol{\beta}_n, \boldsymbol{\beta}_l) \quad \forall (\boldsymbol{\beta}_n, \boldsymbol{\beta}_l) \in \mathcal{C}, \quad (5)$$

where

$$\begin{aligned} Q(\boldsymbol{\sigma}_n, \boldsymbol{\sigma}_l; \boldsymbol{\beta}_n, \boldsymbol{\beta}_l) &= (\mathbf{v}_n(\boldsymbol{\sigma}_n) - \mathbf{v}_l(\boldsymbol{\sigma}_l), \mathbf{v}_n(\boldsymbol{\beta}_n) - \mathbf{v}_l(\boldsymbol{\beta}_l))_{*,o}, \\ F(\boldsymbol{\beta}_n, \boldsymbol{\beta}_l) &= -(\mathbf{u}_n^0 - \mathbf{u}_l^0, \mathbf{v}_n(\boldsymbol{\beta}_n) - \mathbf{v}_l(\boldsymbol{\beta}_l))_{*,o}. \end{aligned}$$

The well-posedness of (2) is a consequence of the following important assumption.

Assumption 2.1. [Strong Cauchy-Schwarz (CS) inequality] *There exists a positive constant $\kappa < 1$ such that for all $(\boldsymbol{\sigma}_n, \boldsymbol{\sigma}_l) \in \mathcal{C}$*

$$|(\mathbf{v}_n(\boldsymbol{\sigma}_n), \mathbf{v}_l(\boldsymbol{\sigma}_l))_{*,o}| < \kappa \|\mathbf{v}_n(\boldsymbol{\sigma}_n)\|_{*,o} \|\mathbf{v}_l(\boldsymbol{\sigma}_l)\|_{*,o}. \quad (6)$$

This assumption, though strong, is reasonable in the context of multiscale modeling; in fact, it holds for problems such as nonlocal diffusion models [?, ?] and multiscale elliptic problems with highly oscillatory coefficients [?].

The following lemma establishes a fundamental property of Q .

Lemma 2.1. *If Assumption 2.1 holds, the form $Q(\cdot, \cdot)$ defines an inner product on \mathcal{C} .*

Proof. The bilinear form $Q(\cdot, \cdot)$ is symmetric and positive semi-definite. We show that it defines an inner product, by showing that $Q(\boldsymbol{\sigma}_n, \boldsymbol{\sigma}_l; \boldsymbol{\sigma}_n, \boldsymbol{\sigma}_l) = 0$ if and only if $(\boldsymbol{\sigma}_n, \boldsymbol{\sigma}_l) = (\mathbf{0}, \mathbf{0})$. Clearly, if $(\boldsymbol{\sigma}_n, \boldsymbol{\sigma}_l) = (\mathbf{0}, \mathbf{0})$ then $\mathbf{v}_n(\boldsymbol{\sigma}_n) = \mathbf{0}$ and $\mathbf{v}_l(\boldsymbol{\sigma}_l) = \mathbf{0}$, implying $Q(\boldsymbol{\sigma}_n, \boldsymbol{\sigma}_l; \boldsymbol{\sigma}_n, \boldsymbol{\sigma}_l) = 0$. On the other hand, if $Q(\boldsymbol{\sigma}_n, \boldsymbol{\sigma}_l; \boldsymbol{\sigma}_n, \boldsymbol{\sigma}_l) = 0$,

$$\begin{aligned} 0 &= Q(\boldsymbol{\sigma}_n, \boldsymbol{\sigma}_l; \boldsymbol{\sigma}_n, \boldsymbol{\sigma}_l) = \|\mathbf{v}_n(\boldsymbol{\sigma}_n) - \mathbf{v}_l(\boldsymbol{\sigma}_l)\|_{*,\mathbf{o}}^2 \\ &= \|\mathbf{v}_n(\boldsymbol{\sigma}_n)\|_{*,\mathbf{o}}^2 + \|\mathbf{v}_l(\boldsymbol{\sigma}_l)\|_{*,\mathbf{o}}^2 - 2(\mathbf{v}_n(\boldsymbol{\sigma}_n), \mathbf{v}_l(\boldsymbol{\sigma}_l))_{*,\mathbf{o}} \\ &\geq (1 - \kappa)(\|\mathbf{v}_n(\boldsymbol{\sigma}_n)\|_{*,\mathbf{o}}^2 + \|\mathbf{v}_l(\boldsymbol{\sigma}_l)\|_{*,\mathbf{o}}^2), \end{aligned}$$

where the last step is a consequence of the strong CS inequality (6) and the Young's inequality. Since $\kappa < 1$ we have

$$(\|\mathbf{v}_n(\boldsymbol{\sigma}_n)\|_{*,\mathbf{o}}^2 + \|\mathbf{v}_l(\boldsymbol{\sigma}_l)\|_{*,\mathbf{o}}^2) \leq 0.$$

Thus, we have that $\mathbf{v}_n(\boldsymbol{\sigma}_n) = \mathbf{0}$ and $\mathbf{v}_l(\boldsymbol{\sigma}_l) = \mathbf{0}$, which implies $(\boldsymbol{\sigma}_n, \boldsymbol{\sigma}_l) = (\mathbf{0}, \mathbf{0})$. \square

Note that to establish the well-posedness of problem (2) we need the completeness of \mathcal{C} with respect to the norm induced by Q . However, this may not be the case; thus, as done in [?], we may consider the completion of \mathcal{C} and solve the optimization problem in the completed space, which we denote by \mathcal{C}_c . Then, we use the Hahn-Banach theorem to extend Q and F in \mathcal{C}_c in a continuous and unique way and we denote the extensions by Q_c and F_c . The latter are such that Q_c is continuous and coercive and F_c is continuous in \mathcal{C}_c . The following theorem is a consequence of the considerations above.

Theorem 2.1. *If Assumption 2.1 holds, the optimization problem (2) has a unique solution $(\boldsymbol{\nu}_n^*, \boldsymbol{\nu}_l^*) \in \mathcal{C}_c$ satisfying the extended Euler-Lagrange equation*

$$Q_c(\boldsymbol{\nu}_n^*, \boldsymbol{\nu}_l^*; \boldsymbol{\beta}_n, \boldsymbol{\beta}_l) = F_c(\boldsymbol{\beta}_n, \boldsymbol{\beta}_l) \quad \forall (\boldsymbol{\beta}_n, \boldsymbol{\beta}_l) \in \mathcal{C}_c.$$

3 The state models and their properties

Let $\Omega \subset \mathbb{R}^3$ be a bounded body with boundary $\partial\Omega = \Gamma$, the peridynamic equation of the displacement of a material point $\mathbf{x} \in \Omega$ at time $t \geq 0$ is given by

$$\rho(\mathbf{x}, t) \frac{\partial^2 \mathbf{u}}{\partial t^2}(\mathbf{x}, t) = \int_{\Omega} \{ \mathbf{T}[\mathbf{x}, t] \langle \mathbf{x}' - \mathbf{x} \rangle - \mathbf{T}[\mathbf{x}', t] \langle \mathbf{x} - \mathbf{x}' \rangle \} dV_{\mathbf{x}'} + \mathbf{b}(\mathbf{x}, t),$$

where $\rho : \Omega \times \mathbb{R}^+ \rightarrow \mathbb{R}^+$ is the mass density, $\mathbf{u} : \Omega \times \mathbb{R}^+ \rightarrow \mathbb{R}^3$ is the displacement field, $\mathbf{b} : \Omega \times \mathbb{R}^+ \rightarrow \mathbb{R}^3$ is a given body force density and $\mathbf{T} : \Omega \times \mathbb{R}^+ \rightarrow \mathbb{R}^{(3,3)}$ is the force state field, i.e, the force state at (\mathbf{x}, t) mapping the bond $\langle \mathbf{x}' - \mathbf{x} \rangle$ to force per unit volume squared. In this work we consider the peridynamic equilibrium equation for a static problem:

$$-\mathcal{L}[\mathbf{u}](\mathbf{x}) := - \int_{\Omega} \{ \mathbf{T}[\mathbf{x}]\langle \mathbf{x}' - \mathbf{x} \rangle - \mathbf{T}[\mathbf{x}']\langle \mathbf{x} - \mathbf{x}' \rangle \} dV_{\mathbf{x}'} = \mathbf{b}(\mathbf{x}). \quad (7)$$

According to the nonlocal theory, we make the assumption that a material point \mathbf{x} interacts only with a neighborhood of points; more specifically, with material points in a ball of radius δ centered in \mathbf{x} , i.e.

$$B_{\delta}(\mathbf{x}) = \{ \mathbf{x}' \in \Omega : |\mathbf{x} - \mathbf{x}'| \leq \delta \},$$

where δ is a length scale referred to as *horizon*. This implies that

$$\mathbf{T}[\mathbf{x}]\langle \mathbf{x}' - \mathbf{x} \rangle = 0, \quad \forall \mathbf{x}' \notin B_{\delta}(\mathbf{x}).$$

We solve (7) in $\omega \in \Omega$ and we prescribe Dirichlet volume constraints in a volumetric layer η surrounding ω so that the entire problem domain is $\Omega = \omega \cup \eta$, see Fig. 1, right. The definition of η depends on the properties of \mathbf{T} and its thickness has to be large enough to guarantee the well-posedness of the problem; we provide more details below. In this work, for simplicity, we consider the linearized linear peridynamic solid (LPS) model [?] characterized by the force state field

$$\mathbf{T}[\mathbf{x}]\langle \boldsymbol{\xi} \rangle = \frac{w(|\boldsymbol{\xi}|)}{m} \left\{ (3K - 5G) \theta(\mathbf{x}) \boldsymbol{\xi} + 15G \frac{\boldsymbol{\xi} \otimes \boldsymbol{\xi}}{|\boldsymbol{\xi}|^2} (\mathbf{u}(\mathbf{x} + \boldsymbol{\xi}) - \mathbf{u}(\mathbf{x})) \right\}, \quad \forall \mathbf{x} \in \Omega, \quad (8)$$

where $\boldsymbol{\xi} = \mathbf{x}' - \mathbf{x}$. Here K is the bulk modulus and G is the shear modulus. The linearized nonlocal dilatation, $\theta : \Omega \rightarrow \mathbb{R}$, is defined as

$$\theta(\mathbf{x}) = \frac{3}{m} \int_{B_{\delta}(\mathbf{0})} w(|\boldsymbol{\zeta}|) \boldsymbol{\zeta} \cdot (\mathbf{u}(\mathbf{x} + \boldsymbol{\zeta}) - \mathbf{u}(\mathbf{x})) dV_{\boldsymbol{\zeta}}, \quad \text{with } m = \int_{B_{\delta}(\mathbf{0})} w(|\boldsymbol{\zeta}|) |\boldsymbol{\zeta}|^2 dV_{\boldsymbol{\zeta}}.$$

Here, the spherical influence function w is a scalar valued function used to determine the support of force states and to modulate the bond strength [?, ?]. Using the linearized LPS force state field in (8) we formulate the three-dimensional peridynamic problem as follows. Find $\mathbf{u} \in [L^2(\Omega)]^3$ such that

$$\begin{cases} -\mathcal{L}_{\text{LPS}}[\mathbf{u}](\mathbf{x}) = \mathbf{b}(\mathbf{x}) & \mathbf{x} \in \omega \\ \mathbf{u}(\mathbf{x}) = \mathbf{g}(\mathbf{x}) & \mathbf{x} \in \eta, \end{cases} \quad (9)$$

where $\mathbf{g} \in [L^2(\eta)]^3$ is a given displacement function and \mathcal{L}_{LPS} is obtained by substituting (8) into \mathcal{L} , i.e.

$$\begin{aligned} \mathcal{L}_{\text{LPS}}[\mathbf{u}](\mathbf{x}) := & \int_{B_\delta(\mathbf{0})} \frac{w(|\boldsymbol{\xi}|)}{m} \left\{ (3K - 5G)(\theta(\mathbf{x}) + \theta(\mathbf{x} + \boldsymbol{\xi}))\boldsymbol{\xi} \right. \\ & \left. + 30G \frac{\boldsymbol{\xi} \otimes \boldsymbol{\xi}}{|\boldsymbol{\xi}|^2} (\mathbf{u}(\mathbf{x} + \boldsymbol{\xi}) - \mathbf{u}(\mathbf{x})) \right\} dV_{\boldsymbol{\xi}}. \end{aligned} \quad (10)$$

We define the layer η as

$$\eta = \{\mathbf{x}' \in \Omega : |\mathbf{x}' - \mathbf{x}| < 2\delta\} \quad \forall \mathbf{x} \in \Gamma. \quad (11)$$

Note that the thickness is double the size of the horizon; this happens because in order to evaluate the peridynamic operator on a boundary point $\mathbf{x} \in \partial\omega$ we need to evaluate a double integral over $B_\delta(\mathbf{0}) \times B_\delta(\mathbf{0})$, i.e. we need values of the displacement in $B_{2\delta}(\mathbf{x})$.

The model (10) has two important features. First, its local limit (i.e. the limit for $\delta \rightarrow 0$, that corresponds to vanishing nonlocal interactions) is the classical Navier-Cauchy equation (NCE) of static elasticity [?]:

$$-\mathcal{L}_{\text{NC}}[\mathbf{u}](\mathbf{x}) := - \left[\left(K + \frac{1}{3}G \right) \nabla(\nabla \cdot \mathbf{u})(\mathbf{x}) + G \nabla^2 \mathbf{u}(\mathbf{x}) \right] = \mathbf{b}(\mathbf{x}), \quad (12)$$

where K , G and \mathbf{b} are defined as in (8). The latter is equivalent to the linear elasticity equation in terms of the Lamé constants (λ, μ) :

$$\begin{aligned} -\nabla \cdot \boldsymbol{\sigma}[\mathbf{u}](\mathbf{x}) &= \mathbf{b}(\mathbf{x}), \quad \text{where} \\ \boldsymbol{\sigma}[\mathbf{u}] &= \lambda(\nabla \cdot \mathbf{u})\mathbf{I} + \mu(\nabla \mathbf{u} + \nabla \mathbf{u}^T) \\ (\lambda, \mu) &= \left(K - \frac{2G}{3}, G \right), \end{aligned} \quad (13)$$

where \mathbf{I} is the identity tensor. This property suggests that the NC model can approximate fairly well the nonlocal model for sufficiently regular solutions; for this reason, it is the local model of choice in our coupling strategy.

Second, for a quadratic displacement field the linearized LPS reduces to the classical NCE (see Proposition 1 in [?]). This property allows us to perform a quadratic patch test, see Section 6.1.

4 Optimization-based LtN formulation of linearized linear peridynamic solid and classical elasticity.

Given a domain Ω representing a bounded body, we introduce a partition into a nonlocal subdomain Ω_n and a local subdomain Ω_l , with boundary Γ_l , such that $\Omega_n = \omega_n \cup \eta_n$ and $\Omega_n \cap \Omega_l = \Omega_o \neq \emptyset$; see Fig. 2 for a two-dimensional illustration.

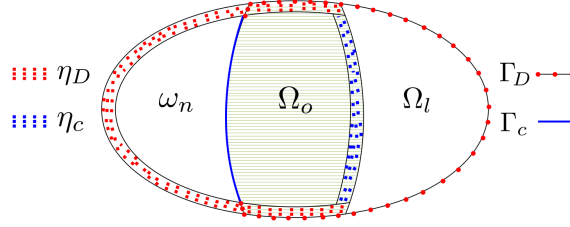


Fig. 2: An example LtN domain configuration in two-dimensions.

We assume that the nonlocal model (10) accurately describes the material behavior in Ω_n while the local NC model gives a fairly reasonable representation for the rest of the domain. We formulate the coupling as an optimization problem where we minimize the difference between the nonlocal and the local solutions on the overlap Ω_o adjusting their values on the virtual interaction volume η_c and the virtual boundary Γ_c determined by the partition. Let $\eta_D = \eta \cap \eta_n$ and $\Gamma_D = \Gamma \cap \Gamma_l$ be the physical interaction volume and boundary where we prescribe the given Dirichlet data, we define the virtual control volume and boundary as $\eta_c = \eta_n \setminus \eta_D$ and $\Gamma_c = \Gamma_l \setminus \Gamma_D$. By posing the peridynamic problem on ω_n and the NC problem on Ω_l we obtain

$$\left\{ \begin{array}{ll} -\mathcal{L}_{\text{LPS}}[\mathbf{u}_n](\mathbf{x}) = \mathbf{b}(\mathbf{x}) & \mathbf{x} \in \omega_n \\ \mathbf{u}_n(\mathbf{x}) = \mathbf{g}(\mathbf{x}) & \mathbf{x} \in \eta_D \\ \mathbf{u}_n(\mathbf{x}) = \boldsymbol{\nu}_n(\mathbf{x}) & \mathbf{x} \in \eta_c \end{array} \right\} \left\{ \begin{array}{ll} -\mathcal{L}_{\text{NC}}[\mathbf{u}_l](\mathbf{x}) = \mathbf{b}(\mathbf{x}) & \mathbf{x} \in \Omega_l \\ \mathbf{u}_l(\mathbf{x}) = \mathbf{g}(\mathbf{x}) & \mathbf{x} \in \Gamma_D \\ \mathbf{u}_l(\mathbf{x}) = \boldsymbol{\nu}_l(\mathbf{x}) & \mathbf{x} \in \Gamma_c, \end{array} \right. \quad (14)$$

where $\boldsymbol{\nu}_n \in [L^2(\eta_c)]^3$ and $\boldsymbol{\nu}_l \in [H^{1/2}(\Gamma_c)]^3$ are undetermined volume constraints and boundary conditions. In our formulation (14) serve as constraints and $(\boldsymbol{\nu}_n, \boldsymbol{\nu}_l)$ as control variables of the optimization problem

$$\min_{\mathbf{u}_n, \mathbf{u}_l, \boldsymbol{\nu}_n, \boldsymbol{\nu}_l} \mathcal{J}(\mathbf{u}_n, \mathbf{u}_l) = \frac{1}{2} \int_{\Omega_o} |\mathbf{u}_n - \mathbf{u}_l|^2 d\mathbf{x} \quad \text{subject to (14)}. \quad (15)$$

Given the optimal controls $\boldsymbol{\nu}_n^*$ and $\boldsymbol{\nu}_l^*$, we define the coupled solution as

$$\mathbf{u}^* = \begin{cases} \mathbf{u}_n^* & \mathbf{x} \in \Omega_n \\ \mathbf{u}_l^* & \mathbf{x} \in \Omega_l, \end{cases} \quad (16)$$

where $\mathbf{u}_n^* = \mathbf{u}_n(\boldsymbol{\nu}_n^*)$ and $\mathbf{u}_l^* = \mathbf{u}_l(\boldsymbol{\nu}_l^*)$.

5 Discretization of the LtN formulation

For the discretization of the NC model in (12) we consider the standard finite element (FE) method. We denote the vector of values of the local discrete solution at the FE degrees of

freedom by $\vec{\mathbf{u}}_l = [\vec{u}_l^1, \vec{u}_l^2, \vec{u}_l^3]$, with $\vec{u}_l^k \in \mathbb{R}^{N_l}$ where N_l is the number of degrees of freedom of each spatial component over the FE computational mesh.

For the peridynamic model introduced in Section 3 we utilize a meshfree discretization. For every point \mathbf{x}_i discretizing the body Ω we approximate the integral operator as follows

$$L[\mathbf{x}_i] := \sum_{j \in \mathcal{F}_i} \{ \mathbf{T}[\mathbf{x}_i] \langle \mathbf{x}_j - \mathbf{x}_i \rangle - \mathbf{T}[\mathbf{x}_j] \langle \mathbf{x}_i - \mathbf{x}_j \rangle \} V_j^{(i)}, \quad (17)$$

where \mathbf{x}_i and $V_j^{(i)}$ are quadrature points and weights and \mathcal{F}_i represents the set of all points in Ω interacting with the i th material point. Note that the quadrature point \mathbf{x}_j is chosen to coincide with the reference position of the j th node; the quadrature weight $V_j^{(i)}$ is the volume of the intersection between the neighborhood of \mathbf{x}_j and the neighborhood of \mathbf{x}_i , i.e. $|B_\delta(\mathbf{x}_j) \cap B_\delta(\mathbf{x}_i)|$. For \mathbf{x}_j near the boundary of $B_\delta(\mathbf{x}_i)$, $V_j^{(i)}$ represents a partial volume. Details regarding the computation of $V_j^{(i)}$ can be found in [?]. We denote the vector of values of the discrete nonlocal solution at the material points by $\vec{\mathbf{u}}_n = [\vec{u}_n^1, \vec{u}_n^2, \vec{u}_n^3]$, with $\vec{u}_n^k \in \mathbb{R}^{N_n}$, where N_n is the number of material points.

We let $S_n \in \mathbb{R}^{N_o, N_n}$ be the matrix that selects the components of \vec{u}_n^k in Ω_o and $S_l \in \mathbb{R}^{N_o, N_l}$ be the operator that evaluates \vec{u}_l^k at the material points in Ω_o ; we define them as

$$(S_n)_{ij} := \delta_{ij} \quad \text{and} \quad (S_l)_{ij} := \phi_j(\mathbf{x}_i), \quad \forall \mathbf{x}_i \in \Omega_o,$$

where ϕ_j is the j th FE basis function.

We define the discrete functional as

$$J_d(\vec{\mathbf{u}}_n, \vec{\mathbf{u}}_l) = \frac{1}{2} \sum_{i=1}^{N_o} \sum_{k=1}^3 |(S_n \vec{u}_n^k)_i - (S_l \vec{u}_l^k)_i|^2 \tilde{V}_i, \quad (18)$$

where \tilde{V}_i is the volume associated with the i th material point, properly scaled.

5.1 Software

The example simulations are carried out using the *Albany* [?] (available at the public git repository <https://github.com/gahansen/Albany>) and *Peridigm* [?] (available at the public git repository <https://github.com/peridigm/peridigm>) codes, developed in the Center for Computing Research at Sandia National Laboratories. *Albany* is a FE code for simulating a variety of physical processes governed by PDEs. It is applied for the majority of the computation, including FE assembly for the Navier-Cauchy equation, calculation of the functional and its derivative, and solution of the state and adjoint systems. *Peridigm* is a peridynamics code for solid mechanics. A software interface was developed to facilitate the linking of *Peridigm* routines with *Albany*; both *Albany* and *Peridigm* rely on several *Trilinos* packages (available

at: <https://trilinos.org/packages>), for example, *Epetra* for the management of parallel data structures, *Intrepid2* for FE assembly, and *Ipack* and *AztecOO* for the preconditioning and solution of linear systems. We apply the LBFGS optimization algorithm, as implemented in the *Trilinos* package *ROL* (available at: <https://trilinos.org/packages/rol>).

6 Numerical tests

In this section we demonstrate the effectiveness of our strategy through several numerical examples. We first show that the OBC method passes linear and quadratic patch tests. In these cases, the analytic solutions are available and are in agreement for the nonlocal and local models. We then apply the OBC approach to test cases in which a discontinuity is present in the nonlocal domain. For these simulations, while the nonlocal and local models behave similarly, differences in their solutions are expected in the overlap domain. We model a rectangular bar containing a crack, followed by a tensile test specimen containing a crack. The latter case represents a realistic engineering geometry that fully exercises the OBC approach in three dimensions.

6.1 Patch tests

The patch test simulations demonstrate the effectiveness of the OBC approach on benchmark problems for which the analytic solutions are available. As mentioned previously, it was shown in [?] that equations (9) and (12) are equivalent for linear and quadratic displacements. As a result, for this class of problem, it is expected that numerical results obtained using the OBC approach should exhibit an excellent match between the local and nonlocal models in the overlap region, with discretization error being the only source of discrepancy.

We consider a rectangular bar in three dimensions:

$$\Omega = [0.0, 100.0] \times [-12.5, 12.5] \times [-12.5, 12.5],$$

$$\omega_n \cup \eta_D \cup \eta_c = [0.0, 62.5] \times [-12.5, 12.5] \times [-12.5, 12.5],$$

$$\Omega_l = [37.5, 100.0] \times [-12.5, 12.5] \times [-12.5, 12.5].$$

Following the configuration illustrated in Fig. 2, the nonlocal domains are constructed such that ω_n is fully encapsulated by $\eta_D \cup \eta_c$. The external layer provided by the domain $\eta_D \cup \eta_c$, in which volume constraints are prescribed, has a thickness equal to twice the horizon (see Section 3). In Fig. 3, nodal volumes on the left and the FE mesh on the right represent the discretizations of $\omega_n \cup \eta_D \cup \eta_c$ and Ω_l , respectively. Further, we define

$$\text{Linear: } \mathbf{u}(\mathbf{x}) = 10^{-3}(x, 0, 0), \mathbf{b}(\mathbf{x}) = \mathbf{0}, \mathbf{g}(\mathbf{x}) = \mathbf{u}(\mathbf{x}),$$

$$\text{Quadratic: } \mathbf{u}(\mathbf{x}) = 10^{-5}(x^2, 0, 0), \mathbf{b}(\mathbf{x}) = \mathbf{b}_q, \mathbf{g}(\mathbf{x}) = \mathbf{u}(\mathbf{x}).$$

We assign to the bulk modulus, K , a value of 150.0, and we assign to the shear modulus, G , a value of 81.496, which are representative of stainless steel. The peridynamic horizon in

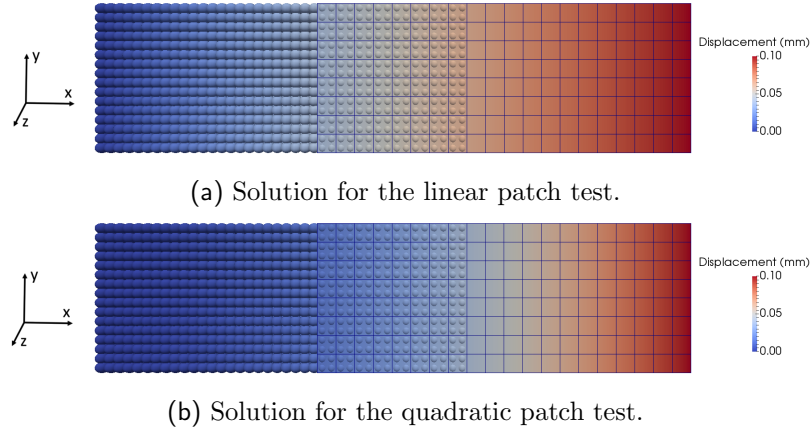


Fig. 3: Solutions for displacement in the x direction for the linear and quadratic patch tests.

the nonlocal domain is assigned a value of 4.270. Following [?], the body force density, \mathbf{b}_q , producing equilibrium under the given quadratic displacement field is given by

$$\mathbf{b}_q = 10^{-5} \left(\frac{8G}{3} + 2K \right) = 5.173.$$

Simulation results for the linear and quadratic patch tests are presented in Figs. 3 and 4. Displacement solutions in the x (horizontal) direction are given in Fig. 3. In Fig. 4, we report the same variable along a horizontal line passing through the center of the bar. The patch test results are in good agreement with the expected linear and quadratic solutions, respectively, for both the nonlocal and local models.

6.2 Rectangular bar with a crack

We next consider a rectangular bar containing a discontinuity (crack) at its center. As illustrated in Fig. 5, OBC is utilized to connect a nonlocal domain covering the center portion of the bar with two local domains located at the ends of the bar. Under this configuration, the discontinuity is contained within the nonlocal domain, and the regions over which (non-control) Dirichlet boundary conditions are applied are restricted to the local domain. This is advantageous because, in practice, the determination and application of nonlocal volume constraints can be problematic [?]. We define the bounded body as

$$\Omega := [-50.0, 50.0] \times [-12.5, 12.5] \times [-12.5, 12.5].$$

The discontinuity is inserted into the geometry via a rectangular plane defined by $x = 0.0$, $5.0 \leq y \leq 12.5$, and $-12.5 \leq z \leq 12.5$. The nonlocal and local domains are defined as

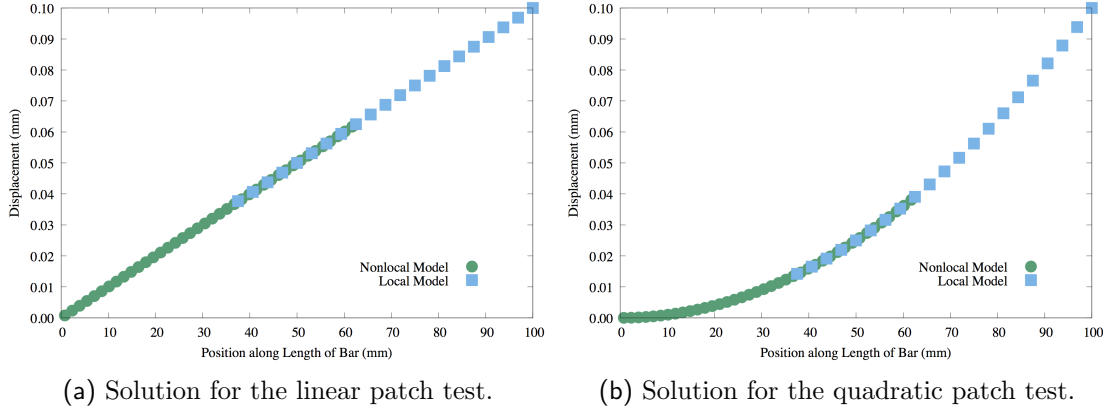


Fig. 4: Solutions for the x component of displacement along a horizontal line passing through the center of the bar for the linear and quadratic patch tests.

$$\omega_n \cup \eta_D \cup \eta_c := [-46.875, 46.875] \times [-12.5, 12.5] \times [-12.5, 12.5],$$

$$\Omega_{l_1} := [-50.0, -34.375] \times [-12.5, 12.5] \times [-12.5, 12.5],$$

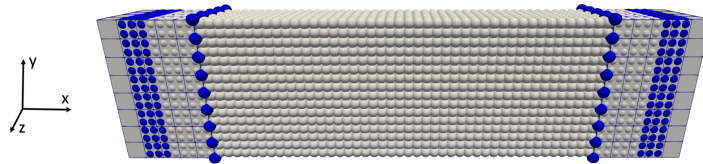
$$\Omega_{l_2} := [34.375, 50.0] \times [-12.5, 12.5] \times [-12.5, 12.5],$$

The domain η_c , over which control Dirichlet conditions for the nonlocal domain are applied, is defined by $-46.875 \leq x \leq -42.1875$ and $42.1875 \leq x \leq 46.875$. The control Dirichlet conditions for the local model are applied to Γ_c , defined by the planes $x = -34.375$ and $x = 34.375$. The locations of the control nodes in the discretized model are highlighted in Fig. 5a. As in the patch tests, the bulk modulus, K , is assigned a value of 150.000 and the shear modulus, G , a value of 81.496. The peridynamic horizon in the nonlocal domain is assigned a value of 2.707. Tensile loading is applied to the bar by prescribing displacements of -0.05 and 0.05 in the x (longitudinal) direction on the faces located at the ends of the bar defined by $x = -50.0$ and $x = 50.0$, respectively. To eliminate rigid body modes, additional zero displacement boundary conditions are applied in the y direction along the edges defined by $x = -50.0, y = -12.5$ and $x = 50.0, y = -12.5$, and in the z direction along the edges defined by $x = -50.0, z = -12.5$ and $x = 50.0, z = -12.5$.

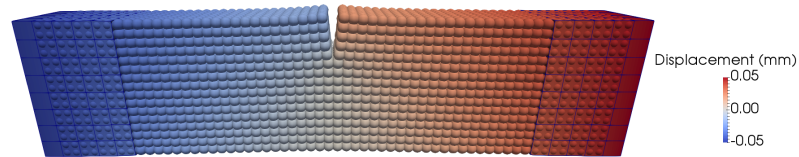
Simulation results are presented in Fig. 5. The three-dimensional image in Fig. 5b shows the opening of the crack that results from tensile loading. Fig. 5c gives displacement results along a horizontal line located on the top face of the bar.

6.3 Tensile test specimen with a crack

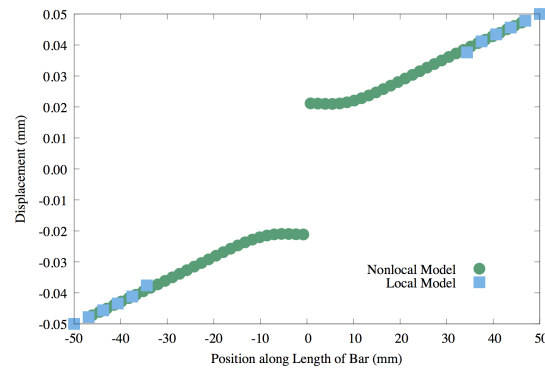
The simulation of a tensile bar with a crack at its midpoint demonstrates OBC for the modeling of a common engineering geometry. As shown in Fig. 6, we restrict the use of the



(a) Discretization for the rectangular bar with a crack. Control nodes are highlighted in blue.

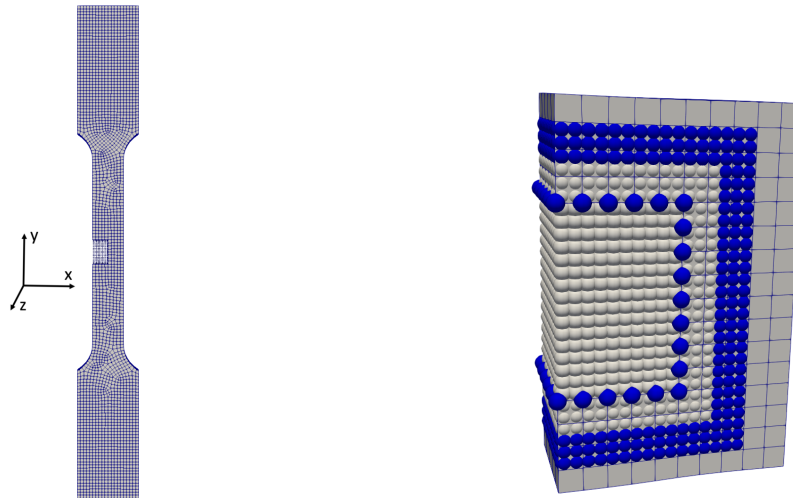


(b) The x component of the displacement solution. Deformation is magnified by a factor of 20 to clearly illustrate the discontinuity.



(c) The x component of the displacement solution along a horizontal line on the top edge of the bar, passing through the discontinuity.

Fig. 5: Discretization and solution for the rectangular bar with a crack.



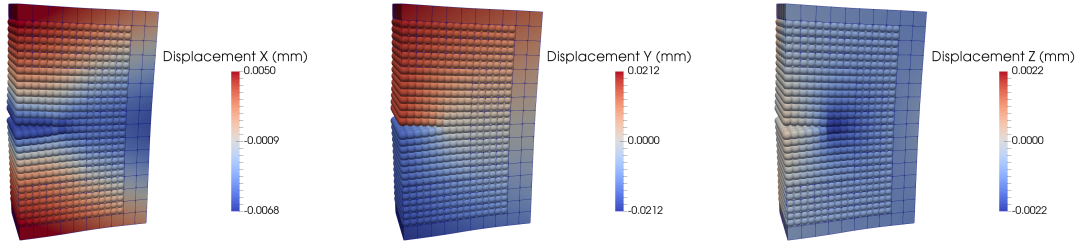
(a) Discretization of tensile bar specimen.

(b) Control nodes in the overlap region.

Fig. 6: Discretization of the tensile bar specimen. The nonlocal domain is restricted to a small subregion near the center of the bar.

nonlocal model to a small subdomain in the direct vicinity of the crack. The overall height of the tensile bar specimen is 100.0 and the width of the bar at its midpoint is 6.25. The nonlocal region, located at the midpoint of the bar and offset to the side of the bar containing the crack, has a height of 8.68 and width of 4.985. The nodes comprising the nonlocal model control domain, η_c , and the local model control domain, Γ_c , are highlighted in blue in Fig. 6b. The discontinuity is inserted via a rectangular plane at the midpoint of the bar extending from the left side of the bar a distance of 1.86 into the bar. We employ material model parameters of 160.0 for the bulk modulus and 64.0 for the shear modulus. For the nonlocal model, the peridynamic horizon is assigned a value of 0.537. Tensile loading is simulated via Dirichlet (displacement) boundary condition applied to the faces at the top and bottom of the bar that produce an overall engineering strain of 0.1% in the y direction. Following the strategy described in Section 6.2, additional zero displacement boundary conditions are applied along edges on the top and bottom faces in the x and z directions to eliminate rigid body modes.

Results for the tensile bar simulation are given in Fig. 7. The influence of the crack on the displacement solution is restricted predominantly to the nonlocal region, and solutions corresponding to the nonlocal and local models are in good general agreement in the overlap domain.



(a) Displacement in x direction. (b) Displacement in y direction. (c) Displacement in z direction.

Fig. 7: Displacement solutions for the tensile test specimen. Deformation is magnified by a factor of 10 to clearly illustrate the discontinuity.

Acknowledgments

This material is based upon work supported by the US DOE's Laboratory Directed Research and Development (LDRD) program at Sandia National Laboratories and the U.S. Department of Energy, Office of Science, Office of Advanced Scientific Computing Research. Part of this research was carried under the auspices of the Collaboratory on Mathematics for Mesoscopic Modeling of Materials (CM4).